Granular Matter (2019) 21:26
https://doi.org/10.1007/s10035-019-0876-8

ORIGINAL PAPER

Modes of wall induced granular crystallisation in vibrational packing

Weijing Dai[1] · Joerg Reimann[2] · Dorian Hanaor[3] · Claudio Ferrero[4] · Yixiang Gan[1]

Received: 22 June 2018

Abstract
Granular crystallisation is an important phenomenon whereby ordered packing structures form in granular matter under vibration. However, compared with the well-developed principles of crystallisation at the atomic scale, crystallisation in granular matter remains relatively poorly understood. To investigate this behaviour further and bridge the fields of granular matter and materials science, we simulated mono-dispersed spheres confined in cylindrical containers to study their structural dynamics during vibration. By applying adequate vibration, disorder-to-order transitions were induced. Such transitions were characterised at the particle scale through bond orientation order parameters. As a result, emergent crystallisation was indicated by the enhancement of the local order of individual particles and the number of ordered particles. The observed heterogeneous crystallisation was characterised by the evolution of the spatial distributions via coarse-graining the order index. Crystalline regimes epitaxially grew from templates formed near the container walls during vibration, here termed *the wall effect*. By varying the geometrical dimensions of cylindrical containers, the obtained crystallised structures were found to differ at the cylindrical wall zone and the planar bottom wall zone. The formed packing structures were quantitatively compared to X-ray tomography results using again these order parameters. The findings here provide a microscopic perspective for developing laws governing structural dynamics in granular matter.

Keywords Granular matter · Packing · Vibration · Boundary effects · Crystallisation

1 Introduction

The behaviour of granular matter subjected to shear, vibration, flow and mixing is of tremendous significance in diverse applications involving the handling and processing of materials in particulate forms [1, 2]. The evolution of granular packing is particularly important as system behaviours and effective properties are closely correlated to packing structure [3]. Recently, granular crystallisation under vibration has drawn increasing interest [4–8]. Like its counterpart in materials science, crystallisation in granular matter can be characterised by the formation of ordered structures. Analogous to heat in materials science, vibration acts as an energy source to agitate particles to jump around and form crystalline structures. However, as granular matter is an athermal and generally repulsive system, the underlying mechanisms differ from bonding at the atomic level. For decades, vibration has been utilised to excite granular matter for fluidisation, segregation and packing [9–12], and is thus utilised in this study to explore how granular crystallisation occurs. Early studies show how internal dynamics of particles determine the macroscopic behaviour of entire granular systems [13, 14]. Depending on the intensity of vibration, macroscopic phenomena manifesting during vibration are compaction [15–17] and convection [18, 19]. However, granular crystallisation lies at the intersection of these two phenomena, as it requires a certain fluidisation to facilitate particle rearrangement yet results in a compacted state.

Experimentally, granular crystallisation has been studied by vibrating existing packings [5, 20] or by adding particles at controlled rates to horizontally or vertically vibrating boxes [4, 21]. In the former scenario, a gradual deceleration

Claudio Ferrero: Deceded on May 25, 2018

✉ Yixiang Gan
yixiang.gan@sydney.edu.au

[1] School of Civil Engineering, The University of Sydney, Sydney, NSW 2006, Australia

[2] Karlsruhe Institute of Technology, P.O. Box 3640, 76021 Karlsruhe, Germany

[3] Fachgebiet Keramische Werkstoffe, Technische Universität Berlin, Berlin, Germany

[4] ESRF-The European Synchrotron, Grenoble, France

Published online: 13 March 2019

of agitation, analogous to annealing, plays an important role in the emergent crystallisation, as do pre-set templates and particular container geometries in the latter case [4]. The use of three-dimensional vibration, rather than uniaxial, is found to further enhance crystallisation by disrupting granular arching [16]. The behaviour of sinusoidal-vibration driven rearrangement of granular packing is manipulated by filling rate and vibration intensity Γ, defined as $\Gamma = A(2\pi f)^2/\mathrm{g}$, where g is the gravitational acceleration, and A and f are the vibration amplitude and frequency, respectively. Maximum crystallisation is found to occur for an intermediate value of Γ [8, 16, 22]. Earlier works have demonstrated the possibility to control granular packing structures through geometry parameters, cohesion and agitation, with the minimisation of internal energy proposed to drive crystallisation. However, a mechanistic understanding of how granular crystallisation occurs and develops under simple and continuous vibration remains elusive. Insights can be gained from the densification of granular matter, where mechanisms have been discussed in terms of the preservation and reconstruction of contact networks [23] and pore size distribution [24].

In order to establish accurate mechanisms, numerical simulations, such as discrete element methods [16, 25] and Monte Carlo methods [8, 11, 17], have been implemented together with X-ray computed tomography (XCT) to examine structural evolution [17] and the appearance of crystalline structures [7]. In recent studies, the emergence of crystallisation by vibration was identified for conditions where the random close packing fraction (0.64) was exceeded [8, 26, 27]. By examining the internal structure of various packings formed under different vibration protocols, the formation of polytetrahedral patterns and octahedral cavities was shown to impart geometrical frustration [7, 28]. Additionally, using high-speed cameras, the role of boundaries in the nucleation of crystalline regimes in two-dimensional systems has been studied across multiple scales in terms of pattern formation and densification as well as their relation to grain mobility [29] and energy dissipation [30]. Three-dimensional systems with planar, convex and concave boundaries have been recently investigated experimentally [27, 31], demonstrating the significance of boundary geometries.

Through well-developed frameworks used to describe analogous crystallisation from glasses or gels in the domain of materials science [32], the field of granular crystallisation remains ripe for further exploration, with a view towards enhancing high-value packing-dependent properties [26, 33]. The present study explores transient states of crystallisation, using a discrete element method (DEM) to simulate dynamic behaviours of vibrated granular matter. Different container geometries were used to examine the boundary influence, with results compared to XCT data. Simulations show that in the absence of cohesion or attraction, granular matter exhibits a clear tendency to crystallise under vibration. Different modes of crystallisation were identified through the analysis on the packing structure transitions. The favoured propagation direction of crystallisation is examined here as a function of container geometry as is the resulting spatial distribution of crystallites.

2 Investigation setup and motivation

2.1 Discrete element method

Dynamics of granular matter subjected to external vibration is simulated by the open source software LIGGGHTS [34] based on DEM. In this method, the propagation of external agitation is interpreted as the result of inter-particle collisions, causing the motion of granular particles. For an individual collision between particles i and j, the normal component $\boldsymbol{F}_{\mathrm{n}}^{i,j}$ and tangential component $\boldsymbol{F}_{\mathrm{t}}^{i,j}$ of the inter-particle force are described by the following equations,

$$\boldsymbol{F}_{\mathrm{n}}^{i,j} = k_{\mathrm{n}}^{i,j}\boldsymbol{\delta}_{\mathrm{n}}^{i,j} - \gamma_{\mathrm{n}}^{i,j}\boldsymbol{v}_{\mathrm{n}}^{i,j}, \quad \boldsymbol{F}_{\mathrm{t}}^{i,j} = k_{\mathrm{t}}^{i,j}\boldsymbol{\delta}_{\mathrm{t}}^{i,j} - \gamma_{\mathrm{t}}^{i,j}\boldsymbol{v}_{\mathrm{t}}^{i,j} \tag{1}$$

where $k_{\mathrm{n}}^{i,j}$ and $\gamma_{\mathrm{n}}^{i,j}$ and ($k_{\mathrm{t}}^{i,j}$ and $\gamma_{\mathrm{t}}^{i,j}$) are contact stiffness and viscoelastic damping coefficient for normal (and tangential) contact, respectively. These quantities are derived from the Hertz-Mindlin contact theory, and thus depend on the instantaneous contact configuration. Here, $\boldsymbol{\delta}_{\mathrm{n}}^{i,j}$ is the overlap distance, $\boldsymbol{v}_{\mathrm{n}}^{i,j}$ and $\boldsymbol{v}_{\mathrm{t}}^{i,j}$ are the relative velocities in the normal and tangential directions, and $\boldsymbol{\delta}_{\mathrm{t}}^{i,j}$ is the tangential displacement vector between particles i and j. In addition, $\boldsymbol{F}_{\mathrm{t}}^{i,j}$ is limited by the Coulomb friction limit, $\left|\boldsymbol{F}_{\mathrm{t}}^{i,j}\right| \leq \mu\left|\boldsymbol{F}_{\mathrm{n}}^{i,j}\right|$, in which μ is the friction coefficient.

2.2 Order characterisation

In the present study, we used void fraction distributions, coordination numbers, contact angle and radial density distributions as well as Voronoi tessellation to characterise the packings [31, 35]. However, we concentrate here on the use of bond orientation order parameters to distinguish crystalline structures and represent the transitions between ordered and disordered states [8, 32]. An advantage of this measure is its insensitivity to particle separation, enabling its use for the transient characterisation of moving granular matter. Together, static and dynamic measures are used to describe the structural changes across order transitions.

Bond orientation order parameters, initially defined by Steinhardt et al. [36], represent the rotational symmetry of sphere assemblies as,

$$Q_{lm}(\vec{r}) \equiv Y_{lm}\left(\theta(\vec{r}), \varphi(\vec{r})\right), \tag{2}$$

where a bond $\vec{r}$ is defined as a vector that points from the centroid of a central particle to one of its neighbour particles, $Y_{lm}(\theta,\varphi)$ are spherical harmonics, $\theta(\vec{r})$ and $\varphi(\vec{r})$ are the polar and azimuthal angles of the bond in a reference spherical coordinates system, and l and m are integers indicating the order of spherical harmonics with the condition that $l \geq 0$ and $|m| \leq l$. By averaging $Q_{lm}(\vec{r})$ over the n_{b}^{i} closest neighbours of a central particle i, the following expression is obtained,

$$\hat{q}_{lm}(i) = \frac{1}{n_{\mathrm{b}}^{i}} \sum_{k=1}^{n_{\mathrm{b}}^{i}} Q_{lm}^{i,k}(k). \tag{3}$$

In the current study, the number of neighbours n_{b}^{i} of a central particle i is selected as 12 [8, 32], the largest coordination number of non-overlapping mono-sized particles, because it gives significantly different feature values between crystalline structures like BCC, HCP, FCC and even icosahedral. Finally, the local bond orientation order for particle i is constructed as [37]

$$Q_{l}^{\mathrm{local}}(i) \equiv \left(\frac{4\pi}{2l+1} \sum_{m=-l}^{l} \left| \hat{q}_{lm}(i) \right|^{2} \right)^{1/2}, \tag{4}$$

$$\hat{W}_{l}(i) = \frac{\sum_{m_1,m_2,m_3} \begin{pmatrix} l & l & l \\ m_1 & m_2 & m_3 \end{pmatrix} \hat{q}_{lm_1}(i)\hat{q}_{lm_2}(i)\hat{q}_{lm_3}(i)}{\left[\sum_{m=-6}^{6} \left| \hat{q}_{lm}(i) \right|^{2} \right]^{3/2}}, \tag{5}$$

where the term in the parentheses is Wigner-3j symbol. $l = 4$ and 6 are widely used due to their unambiguous value for crystalline structures [32, 37].

Order indices of neighbourhood configuration of a central particle i are defined on the basis of a vector $\overrightarrow{\boldsymbol{q}_6}(i) = \left[\hat{q}_{6m}(i)\right]$, with $m = -6, -5, \ldots 0, \ldots 5, 6$. The cosine similarity of a pair of such vectors of neighbouring particles i and j is calculated as

$$\mathrm{CosSimi}(i,j) = \mathbf{Re}\left[\frac{\overrightarrow{\boldsymbol{q}_6}(i)}{|\overrightarrow{\boldsymbol{q}_6}(i)|} \cdot \frac{\overrightarrow{\boldsymbol{q}_6}(j)}{|\overrightarrow{\boldsymbol{q}_6}(j)|} \right] = \mathbf{Re}\left[\frac{\sum_{m=-6}^{6} \hat{q}_{6m}(i) \cdot \hat{q}_{6m}^{*}(j)}{|\overrightarrow{\boldsymbol{q}_6}(i)||\overrightarrow{\boldsymbol{q}_6}(j)|} \right]. \tag{6}$$

$\mathrm{CosSimi}(i,j)$ between particles i and j is positively correlated with the similarity of their individual neighbourhood configurations, and a pair of connected particles has $\mathrm{CosSimi}(i,j) \geq 0.7$ [38]. Hence, the order of individual particles can be positively represented by the parameter [32],

$$S_{6}^{i} = \sum_{j}^{n_{\mathrm{b}}^{i}} \mathrm{CosSimi}(i,j), \tag{7}$$

ranging between 0 and 12. For each particle, high S_{6}^{i} means that particles in an ensemble have similar neighbourhood configurations, characterising local crystalline perfection. Additionally, to describe the overall structural order of an assembly of particles, we make use of [33],

$$F_{6} = \frac{1}{N_{\mathrm{P}}} \sum_{i=1}^{N_{\mathrm{P}}} f_{6}(i), \tag{8}$$

where

$$f_{6}(i) = \frac{1}{n_{\mathrm{b}}^{i}} \sum_{j=1}^{n_{\mathrm{b}}^{i}} \Theta\left[\mathrm{CosSimi}(i,j) - 0.7\right], \tag{9}$$

with the step function $\Theta(\cdot)$. Spanning the range 0–1, the term F_6 is used to characterise the structural evolution during vibration, as an alternative to the conventional packing fraction.

A bottom-up *Coarse-graining* methodology is applied in this work to convert the discrete data set of the order index S_{6}^{i} into a higher-scale continuum form to reveal the spatial distribution of order in the structure. In general, the coarse-graining approach used here takes a set of discrete points $\boldsymbol{P}_i = (x_i, y_i, z_i)$ and their corresponding scalar data h_i as input [39, 40]. Instead of describing the density at any point $\boldsymbol{P} = (x, y, z)$ by $\rho^{\mathrm{dis}}(\boldsymbol{P}) = \sum_i h_i \delta(\boldsymbol{P} - \boldsymbol{P}_i)$ where $\delta(\Delta\boldsymbol{p})$ is the Dirac delta function, the coarse-graining approach transforms this discrete field into a continuous one by replacing $\delta(\Delta\boldsymbol{p})$ with a positive semi-definite function $\varphi(\Delta\boldsymbol{p})$. This function fulfils the requirement that the integral of the continuous density function

$$\rho^{\mathrm{con}}(\boldsymbol{P}) = \sum_{i} h_i \varphi(\boldsymbol{P} - \boldsymbol{P}_i) \tag{10}$$

is equal to the sum of h_i for a given volume. The exact form of $\varphi(\Delta\boldsymbol{p})$ is not determinative but the width w at which $\varphi(\Delta\boldsymbol{p})$ vanishes holds significance [39]. Here, a three-dimensional Gaussian function is employed,

$$\varphi(\boldsymbol{P} - \boldsymbol{P}_i) = \frac{e^{-\frac{1}{2}\left[\left(\frac{x-x_i}{r}\right)^2 + \left(\frac{y-y_i}{r}\right)^2 + \left(\frac{z-z_i}{r}\right)^2\right]}}{(2\pi)^{\frac{3}{2}}}. \tag{11}$$

This function vanishes at $w = 3r$ where r is the radius of particles. This selection of w results from the fact that the order index S_{6}^{i} is based on particle ensembles roughly occupying a spherical region with the radius of 3 r.

2.3 Dynamic characterisation

Granular-temperature is often used as a term, analogous to thermal energy at the atomic scale, to describe the

kinematics of granular matter. While crystallisation and ordering at the atomic scale are studied with respect to thermal conditions, here we examine the local and global ordering of packing with respect to the dynamic status of particles. Granular temperature quantifies the velocity fluctuation of particles in granular matter rather than being a measure of thermal energy [41]. To obtain the granular temperature, granular matter is first discretised into particle ensembles [42]. For each ensemble of n particles, the average velocity is calculated in x, y, and z axis as $\bar{v}_{x,y,z} = \frac{1}{n}\sum_{i=1}^{n} v^i_{x,y,z}$, respectively. Then the velocity fluctuation along x, y, and z axes are derived separately by

$$\mathrm{GT}_{x,y,z} = \frac{1}{n}\sum_{i=1}^{n}\left(v^i_{x,y,z} - \bar{v}_{x,y,z}\right)^2. \tag{12}$$

Finally, the granular temperature is the mean of the three axial granular temperatures $\mathrm{GT} = \frac{1}{3}\left(\mathrm{GT}_x + \mathrm{GT}_y + \mathrm{GT}_z\right)$. Consistently, the ensembles used to derive the granular temperature are chosen as the 12-neighbour configuration used in the S_6 calculation. In this way, every particle has its granular temperature order index S_6, and relationships between granular temperature and granular crystallisation can be investigated.

2.4 Application to experimental observations

The aforementioned order characterisation methods are applied to two previously studied cases of vibrated granular media, both confined by cylindrical boundaries [31]. Exp C (same notation as in [31]) has a slender shape, 30 mm in its cylindrical diameter and 70 mm in its height, and Exp D is relatively flat, 50 mm in diameter and 40 mm in height. The coordinates of their particles were obtained by XCT techniques. One apparent difference between these two granular media is the order of the superficial particles. Exp C shows extensive hexagonal packing on the cylindrical surface and disordered packing on the top surface (Fig. 1a). However, Exp D shows an opposite trend, despite the existence of discontinuous hexagonal packing (Fig. 1b). In order to expose the internal packing of these granular media, the S^i_6 of individual particles are computed and fed into the coarse-graining approach to construct spatial density mappings of S_6, as given by Fig. 1c, d. Since the order of packing is positively related to S_6, the redder region indicates stronger crystallisation. In consistence with the superficial packing of these two granular media, crystallised regions in Exp C and Exp D exhibit radial and axial accumulation, respectively. The redder colour in the mapping of Exp D implies that fewer defects exist in the packing compared with Exp C. This motivates further investigations into the relations between granular crystallisation and geometrical characteristics.

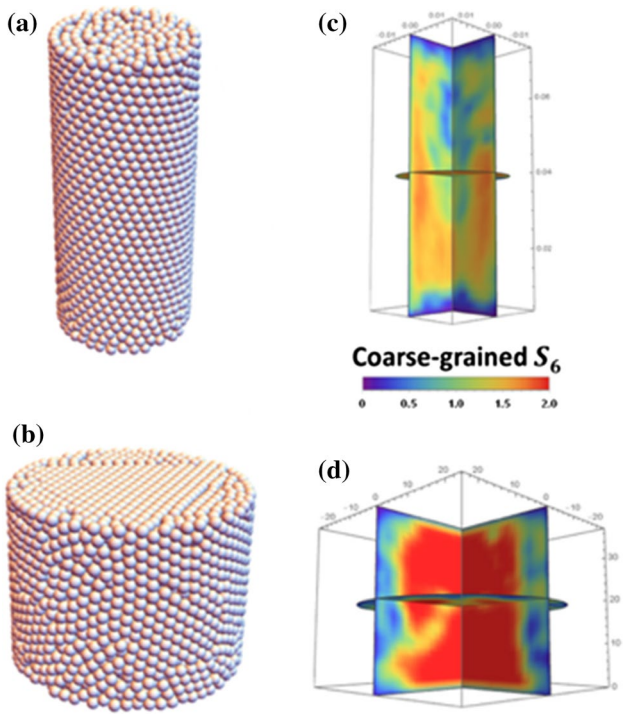

Fig. 1 Reconstruction (left column) and S_6 density mappings (right column) of two vibrated granular media. Exp C-**a** and **c**, Exp D-**b** and **d**

3 Results

3.1 Simulation parameters

To investigate the influence of container boundaries on granular crystallisation, mono-dispersed frictionless spheres were generated in cylindrical containers of different radii and heights. Then, the evolution of the packing structures inside these granular media during continuous sinusoidal vibration was simulated and characterised to study the crystallisation process. The simulations followed a similar scheme. Firstly, 5000 particles of size d were randomly dispersed in a finite cylindrical container with a diameter D and were allowed to settle under gravity. This state was considered as the initial state before vibration. Sinusoidal vibration function with an amplitude A and frequency f was introduced by moving the bottom of the cylindrical container in the axial direction along the gravitational direction. At the upper surface of the granular matter, a lid that could move freely in axial direction confined the granular matter in a negligible pressure of a few Pa. This lid, also used in [31], is particularly used to calculate the packing fraction. The vibration was applied over 1000 periods ($T = 1/f$), followed by sufficient relaxation (1 s) to reach static equilibrium. The vibration amplitude was varied to study the influence of the energy input on the crystallisation. Table 1 summarises the

Table 1 Parameters for DEM simulations

Young's modulus, E	63 (GPa)
Poisson ratio, ν	0.2 (–)
Density, ρ	2230 (kg/m^3)
Friction coefficient, μ	0.0, 0.2, 0.5 (–)
Coefficient of restitution	0.6 (–)
Diameter of sphere, d	2.3 (mm)
Container diameter/height, D/H	30/75, 40/60, 50/25, 60/19 (mm/mm)
	denoted as D30, D40, D50, D60
Vibration amplitude, A	0.23 (0.1 d), 0.46 (0.2 d) (mm)
Vibration frequency, f	50 (Hz)
Gravitational acceleration, g	9.8 (m/s^2)
Vibration intensity, Γ	2.3, 4.6 (–)

material and simulation parameters used in the study. The diameters and the initial heights of the cylindrical volumes were varied to study the geometrical influence on the crystallisation process. $D/H = 30/75$ (with $D/d \approx 13$, $H/d \approx 33$) is characteristic for a rather slender container, while the case $D/H = 60/19$ (with $D/d \approx 26$, $H/d \approx 8$) represents a rather flat one. The chosen geometrical parameters $D/H = 30/75$ and $D/H = 50/25$ are similar to those investigated by XCT [31] for the purpose of reliable comparison between simulation and experiment.

3.2 Selective crystallisation by wall effect and epitaxial growth

By employing DEM simulations to track transient states of particles during vibration, the dynamic development of crystalline structures is unveiled, which supplies information difficult to be obtained by XCT. Following the method introduced in Sect. 2.4, S_6 density mapping is constructed to spatially expose the propagation of the periodic crystalline structures, featured by high S_6 regimes. In the sequential S_6 mappings of the granular media experiencing vibration, the dynamic process of crystallisation is reconstructed by the morphology and intensity evolution as shown in Fig. 2.

The general and common phenomenon appearing in all cases is that the region of high S_6 (shown in red colour) in the density mappings expands and intensifies with vibration, and eventually reaches a quasi-equilibrium state in which only minor changes of ordering could be observed (row by row in Fig. 2). Larger amplitude accelerates the crystallisation rates and produces larger crystalline regimes. In addition, increasing D results in regions of higher S_6 value, indicating finer crystalline regimes. This phenomenon can be explained by the structural difference in those crystalline regimes which will be addressed in later sections. Within the scope of current study, the granular crystallisation is initiated automatically once the vibration commences. It

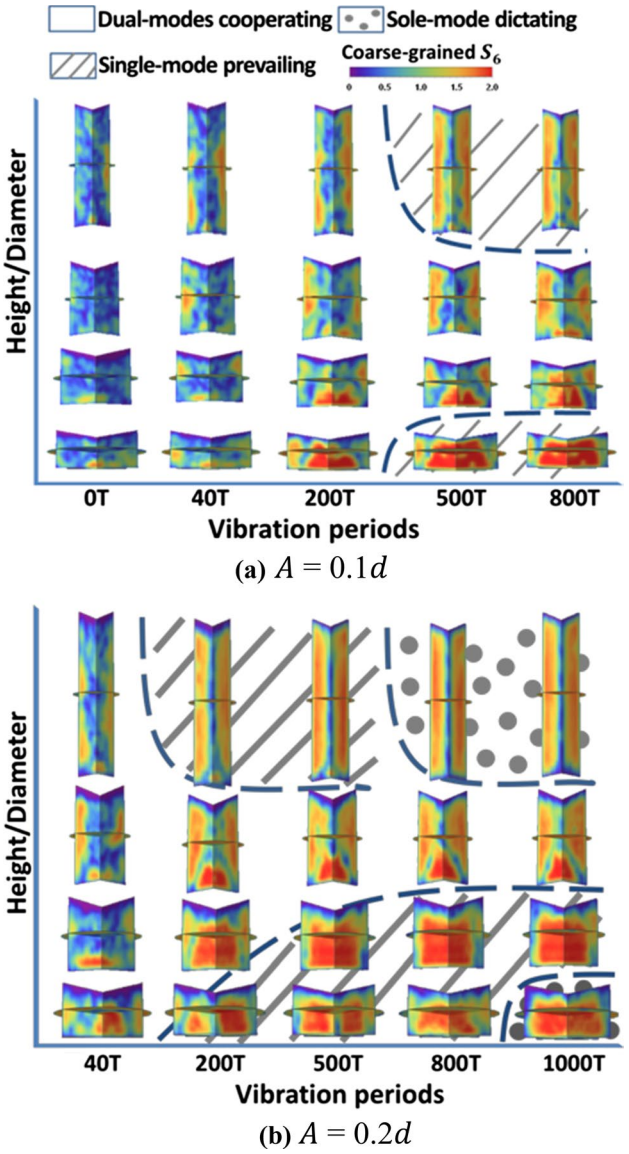

Fig. 2 Evolutional phase diagram of the crystallisation in granular media of different height-to-diameter ratio. Each S_6 density mapping consists of central plane slices of three axes, the colour indicated by coarse grained S_6 suggests disorder in violet direction and crystallisation in reddish direction. In the phase diagrams three phases are marked by background filling, (1) dual-modes cooperating; (2) single-mode prevailing; and (3) sole-mode dictating which are approximately determined by the competition between cylindrical and bottom modes

could be inferred that highly disordered granular matter is vulnerable to dynamic perturbations like vibration, while the crystallised granular matter at the quasi-equilibrium state manifests the stability of crystalline structures.

Regarding the growth of crystalline regimes, a wall effect is identified in all geometries. According to the S_6 density mappings at the early periods, reddish regions indicating highly ordered structure always preferentially appear at the

bottom walls and cylindrical walls (the second column in Fig. 2a and the first column in Fig. 2b). This preferential crystallisation can be partly explained by the existence of a partially ordered layer of particles adjacent to the walls before vibration, which can be seen from the first column in Fig. 2a. These ordered layers emerge during the settlement of granular matter because the particles need to rest in positions with as many contacts as possible to support themselves under frictionless conditions, which also conforms to the inherent partially ordered regions existing at walls in recent XCT data [31]. However, those partially ordered layers can also be developed near the walls during vibration, which highlights the robustness of two-dimensional ordered layers in spite of collisions by other particles. After the similar prior crystallisation at walls, the emerging crystallisation becomes dependent on the container boundary configuration, i.e., D/d and H/d. Subjecting to the origin of the crystalline regimes, two crystallisation modes can be differentiated in this period, the cylindrical mode and the bottom mode. The cylindrical mode induces crystalline regimes in a radially inward direction, whereas crystalline regimes grow upwards along the axial direction in the bottom mode. Thus, a competing mechanism between these two modes is introduced for the subsequent crystalline growth stage, which is determined by the H/D ratio. As the H/d decreases and D/d increases, crystallisation at the bottom wall becomes the favoured mode. Conversely, the cylindrical mode dominates the crystallisation. This trend is responsible for the observed radial and axial accumulation of crystallised regions found in previously reported experimental work, as shown in Sect. 2.4.

Evolutional phase diagrams were constructed by comparing the S_6 density maps of different granular media at the specific vibration duration. Two operational phases exist in the phase diagram of small amplitude ($A = 0.1\ d$) while for the large amplitude ($A = 0.2\ d$) three phases are observed. In the early periods, all granular media exhibit a "dual-mode cooperating" phase where crystallisation progresses on both cylindrical and bottom walls. When the granular media continue to be vibrated, either the cylindrical mode or the bottom mode prevails in crystallisation ("single-mode prevailing" phase), although different crystalline regimes grown in the other modes can still be identified. The exception D40 is always in the dual-mode phase, in which disordered regions act as boundaries and partition different crystalline regimes. The boundary regions are instable because of the mismatch between crystalline regimes grown in two different modes.

Most interestingly, a third operational phase is present for D30 and D60 in the final periods of large amplitude vibration. This phase represents the extreme scenarios where one of the crystallising modes is eliminated, named as "sole-mode dictating" phase. This third operational phase was experimentally observed by one of the authors in the vibrated particle geometries corresponding to D30 but also for Exp D which is representative of large D/d and small H/d. In the latter case, the cylindrical wall layer was fairly hexagonally packed for the longest part of the total vibration period. Then this layer became significantly unstable, resulting finally in a much less ordered wall layer while at the top bed surface a well-defined hexagonal pattern appeared, as shown in Fig. 1b. In the D60 simulation, the "sole-mode dictating" phase is well-developed but exists also for D50 in the final stage.

Figure 3 shows the variation of F_6 in the cylindrical wall layer, the bottom layer and the core region separately with extended vibration periods. Both wall layers possess higher F_6 than the core region at the initial state, proving the existence of partially ordered regimes. Not only for the initial state, has this comparison underlined the significance of the wall effect during the granular crystallisation. The F_6 evolution of the two wall layers conforms the phase separation in the evolution diagrams. In the dual-mode cooperating phase, the contrast between the patterns is small and both parts exhibit a common trend of increase-to-stabilise behaviour. As the contrast extends or a crossover arises, the granular matter moves into the single-mode prevailing phase. Regarding the sole-mode dictating phase, it is foreshadowed by the continuous decrease of the F_6. The decrease of the F_6 proves that those wall layers become disordered by vibration, wiping out the corresponding mode.

Since very large granular systems (particle numbers $\gg 10^4$ [43, 44]) are beyond the aims of the current study, we conclude that granular crystallisation in containers of finite size is initiated by the wall effect and progresses in modes that depend on the wall geometry. The wall effect of both cylindrical and bottom modes generates quasi two-dimensionally ordered layers with as many contacts as possible which we will subsequently prove to be hexagonal packings. The following processes are the expansion of the hexagonal packing across the wall plane and the epitaxial growth of an adjacent layer. The repetition of these stepwise processes establishes the granular crystallisation in these confined systems. Because of imperfections and the competition with other crystallised layers, each epitaxial layer is smaller than the preceding one, resulting in conical crystalline regimes. From an energetic perspective, the underlying microscale mechanism is proposed as the selection of positions with high number of contacts to enhance the propagation of kinetic energy. Owing to the maximised contacts, the kinetic energy induced by the vibration on the one hand dissipates quickly from one particle to its surroundings in such structures, leaving the particle in a less perturbed state and making the crystalline regimes robust; on the other hand, this kinetic energy is efficiently transferred throughout the crystalline arrangements, triggering the relocation of particles from the disordered regions into particular crystallising

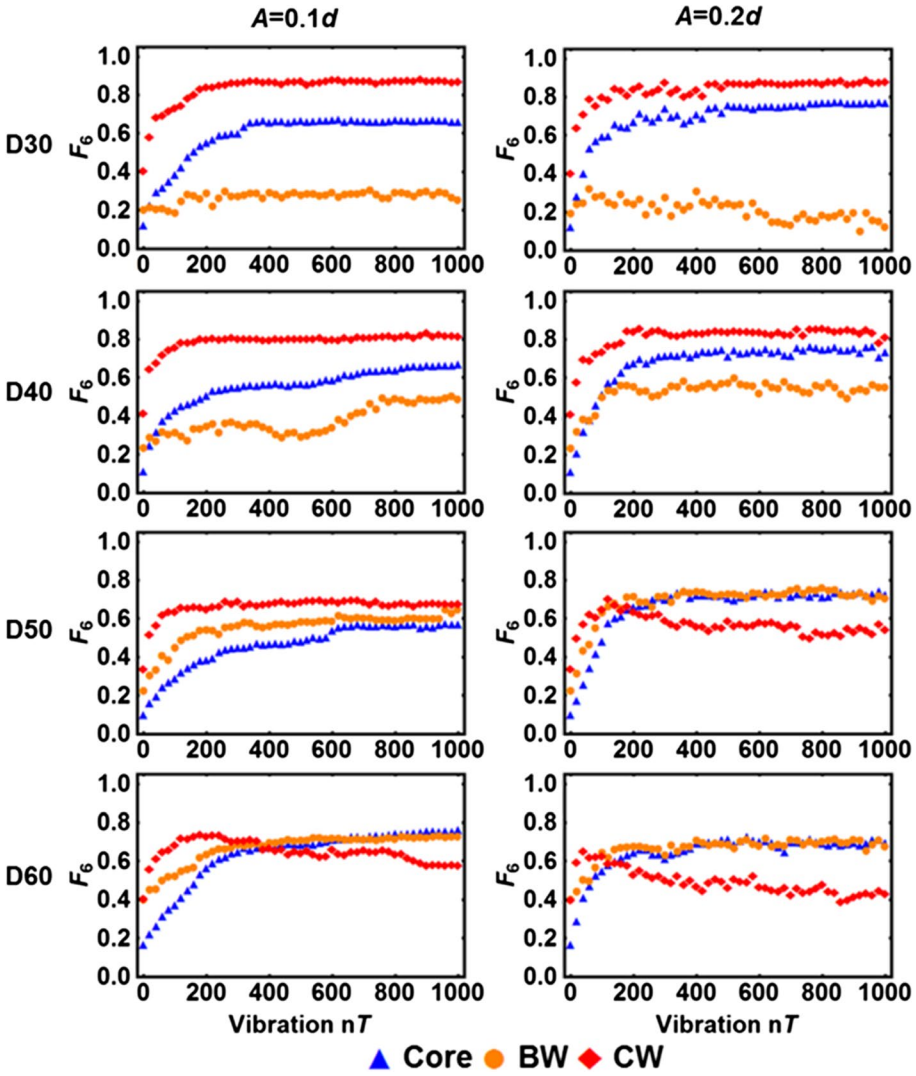

Fig. 3 Evolution of F_6 for particle groups separated by position. CW-first layer near the cylindrical wall, BW-first layer near the bottom wall and core-the bulk particles

positions nearby. Such steps build up a positive feedback loop to promote crystallisation. Therefore, larger amplitude activates more particles near ordered layers and enhances the possibility for these particles to lodge in an energetically favourable position. However, too much energy will reverse those steps, cause drifting particles and deteriorate the crystallisation. Self-nucleation [43] is not the prevailing mechanism due to the repulsive nature of granular matter, while the merging of crystalline regimes is commonly observed in current study.

3.3 Transient state versus static state

In the context of crystallisation in various systems, the interplay between densification and order formation has been debated by researchers to determine whether the densification precedes the order formation or the other way around [45], while some reports suggest that these two processes occurred simultaneously [46]. Densification in granular matter, characterised by static packing fraction (γ) in vibrating-relaxing processes, indicates different stages of granular crystallisation [8, 44], presenting cooperative development between these two aspects. However, according to the temporal evolution of γ and F_6 in the right column in Fig. 4, γ at transient state exhibits fluctuation due to the granular dilation resulted from repulsive interaction, shadowing its relation with the order formation. On the other hand, the order formation, given by the increase of F_6, persists despite the unstable densification. Such decoupling phenomenon stresses that the order formation should be focused when the granular crystallisation is studied in the transient state.

Within the vibration duration in this study, two stages can be distinguished according to the evolution of F_6. The first stage is characterised by the monotonic and rapid increase of F_6, which corresponds to particles in disorder moving into order positions. The second stage can be treated as a quasi-equilibrium state, featured by the mild change of F_6. In other words, this phenomenon suggests that the order formation

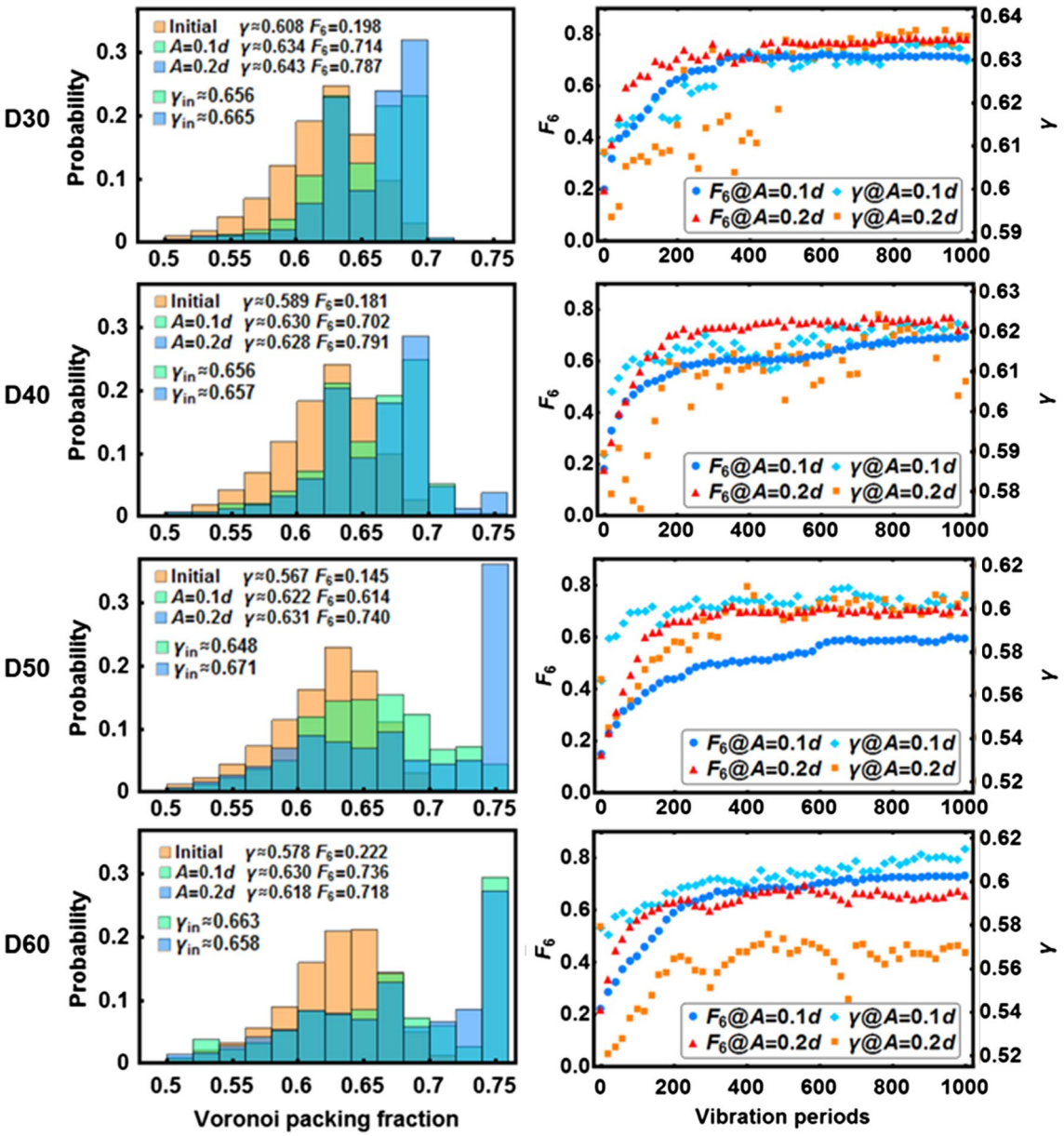

Fig. 4 Overall evolution of each granular medium subjected to vibrations of different amplitude. The histograms (colouring with transparency) in the left column show distributions of the Voronoi cell packing fraction of the initial state and two final relaxed states after vibration ($A=0.1\ d$ and $A=0.2\ d$) with legends giving the corresponding overall packing fraction γ and structural index F_6. The corresponding right column plots demonstrate the time variation of the overall γ and F_6 at transient states during vibration

cannot fully be accomplished by single vibration mode and wall effect must be carefully examined when producing single-crystal granular matter [5, 16]. These are the reasons that the current simulation cannot reach fully crystallised state ($\gamma \geq 0.7$) when compared with other simulation with periodic boundary condition as well as additional lateral perturbation [6, 8].

The static final states of the granular media, including the distributions of the Voronoi cell packing fractions [47], as well as the γ and F_6, are shown in the left columns of Fig. 4. Both γ and F_6 increase in the final relaxed states after vibration. The larger amplitude leads to a bigger increment in γ and F_6 except for the case of D60. This exception can be attributed to the relatively strong fluidisation because of the least gravitational potential to overcome, i.e., the least H. These results are in agreement with previously reported DEM studies [35] and Monte Carlo simulation [8] as well as experiments [31, 48] in which γ and F_6 are maximised at an intermediate vibration intensity. Regarding the Voronoi cell packing fraction distributions, the bell-shape distributions

of all the initial states change into several peaks at the final states. With increasing D and decreasing H, a peak at ≈ 0.74 develops, which proves the emergence of a highly crystallised structure. By excluding the superficial particles of the corresponding granular matter, the internal packing fractions γ_{in} have been given, which is consistent with the proved concept that granular crystallisation occurs with packing fraction larger than RCP ($\gamma \approx 0.64$) [8] as well as the experimental observation for the inner zones of granular media in similar cylindrical containers [27].

3.4 Granular temperature and crystallisation

Analogous to the structural order representing the similarity of neighbour configuration, we consider the uniformity of the velocities of particles in an ensemble as the dynamic order that can be quantitatively described by the granular temperature.

The variation of the S_6 distributions during vibration exhibits a general trend regardless of the geometry, in which a singular peak gradually intensifies, with final states shown in Fig. 5a. Therefore, we make use of the S_6 distributions to examine how the granular temperature evolves under different conditions. By using the particle connection criteria based on the magnitude of S_6, the particles are categorised into two groups, the solid-like and liquid-like [38]. Within the solid-like group, the particles are categorised again into two sub-groups, the highly crystallised and moderately ordered, by setting a threshold for highly crystallised particles, i.e., $S_6 > 10$; because no liquid-like particle possesses S_6 which exceeds 10. Finally, the average granular temperature can be extracted for three groups. As discussed in the previous sections, the particles in the disorder regions are more active than those in the crystallised regimes, thus, suppressing the dynamic order. A general observation is that the highly crystallised particles have the lowest average granular temperature, but the liquid-like particles have the highest average granular temperature. The distinction of D60 vibrated via large oscillation shown in Fig. 5d demonstrates that the dynamic order of crystallised particle is suppressed in the over-fluidised state. Thus, we argue that the granular temperature has a transition from divergence to convergence depending on the geometry and the vibration intensity.

This phenomenon is consistent with the discussion on the relationship between the propagation of kinetic energy and the order formation in the crystallisation presented in the previous sections. Along with the rise of S_6, the local structure of individual particles becomes periodic and symmetric. As a result, the particle collisions inside such crystalline structures turn out to be counterpoised, helping the structures to attain the stability by suppressing velocities deviating from the vibration axis and preventing the particles from over-acceleration. In conclusion, the structural order is the foundation for the dynamic order. The granular crystallisation can stabilise the granular matter subjected to agitation by resetting the elevation of the granular temperature.

3.5 Structural characterisation and evolution

It has been demonstrated in the previous sections that the wall effect and the dual crystallisation modes are the major events during vibration. To further distinguish the structural

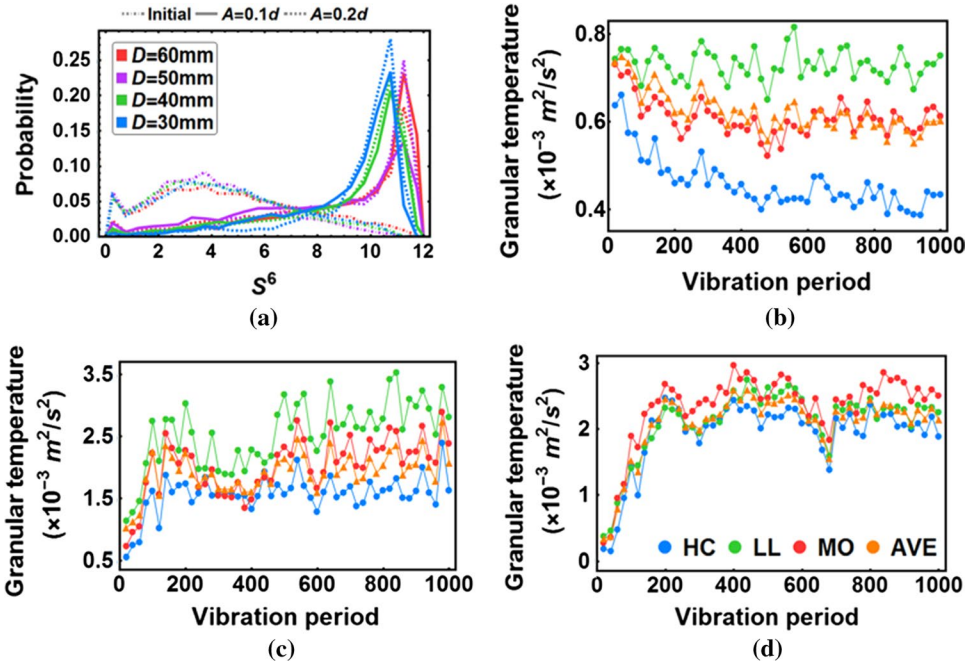

Fig. 5 **a** A similar trend in the S_6 evolution is observed in all cases. The S_6 accumulates between 10 and 12 in the final state, while the peak right shifts as D increases. **b** Typical granular temperature evolution (D50) in the small amplitude vibration scenario. **c** Typical granular temperature evolution (D40) in the large amplitude vibration scenario. **d** Granular temperature evolution in the relatively strong fluidisation case (D60). **b** and **c** have the same legend shown in **d** with HC-highly crystallised, LL-liquid like, MO-moderately ordered, AVE-averaged

types of crystalline regimes, the local bond orientation parameters Q_6^{local}, W_4^{local} and W_6^{local} have been utilised to differentiate. Firstly, W_6^{local} is used to examine whether cubic-based structures exist according to its sign (±) contrast, positive for BCC and negative for HCP and FCC. Nearly all particles have negative W_6^{local}, denoting that most particles sit in hexagon-based structures (not shown explicitly in the figures). This result is consistent with the crystallised structure in granular matter obtained in other research [6, 8, 26], implying that BCC is not the preferential structure in granular crystallisation. Next, the (Q_6^{local}, W_4^{local}) coordinates are employed to specify HCP (0.485, 0.134) and FCC (0.575, −0.159).

In Fig. 6, two series of the probability density distributions of (Q_6^{local}, W_4^{local}) demonstrate the typical development pathways of the crystalline structures in D30 and D60, respectively. The similar broad distribution of the pairs of (Q_6^{local}, W_4^{local}) indicates the initial disordered nature. Three structuring paths are clearly identified in the granular crystallisation. Once the vibration starts, the path leading to a non-typical structure coordinates, neither HCP nor FCC, appears first. Such coordinates, calculated from the neighbour configurations with lack in half space due to the boundary condition, represent the hexagonally packed surface particles in finite HCP or FCC structures. In accordance with the previous discussion, this path preceding over other paths reveals the priority of the tendency towards hexagonal units in the wall layer. When the vibration continues, HCP and FCC become the main structures emerging during crystallisation. As stated before, the dominating crystallisation mode in the granular media of D30 and D60 is the cylindrical mode and the bottom mode, respectively. According to the density contrast in the HCP and FCC paths between D30 and D60, the cylindrical mode shows a preferential selection of the HCP structure, but the bottom mode has less bias on the two paths. The histograms according to probability density function of Q_6^{local} of these granular media at the corresponding snapshots are presented in the rightmost column in Fig. 6 for a more clearly quantitative sense. Differently from most studies implementing periodic boundary conditions [6, 8, 26] or excluding near wall regions [49], not only is the priority of the growth of wall layer identified here, but also the dominance of FCC over HCP is not observed within the vibration cycles in this work, all marked as the significances of the wall effects.

Regarding the cylindrical mode, contributing the formation of HCP structures most in D30 and D40 cases, the distinctive crystalline regime is characterised by a deviation from the perfect HCP coordinates. As demonstrated in Fig. 7a, the resulted structure distortion comprising of HCP segments (blue particles in Fig. 7a) of which W_4^{local} is positive, and rupture particles (yellow particles in Fig. 7a) that are distinguished by their W_4^{local} close to 0. By comparing P1, P2 and P3 in Fig. 7, layer shifts are found in the neighbour configurations of the segment particles, but incomplete layers are the typical feature of those rupture particles. This cylindrical curvature effect, discussed also in [31], causes a decrease of the Voronoi cell packing fraction and the coordination number, as well as weakens the ordering of the crystalline regimes near the cylindrical walls in consistence with Fig. 2.

One possible explanation of this phenomenon can be formed at the stronger mechanical stability of FCC than HCP [50], implying lower resistance of HCP to deform in a distorted field like the cylindrical wall. Thus, this stronger deformability may contribute to the prevalence of HCP in the cylindrical mode. As the distortion becomes smaller with D increasing, more FCC particles appear in the cylindrical wall region as shown later in Fig. 9.

Second, although the difference in mechanical stability helps to explain the HCP dominance in the cylindrical mode, the lack of a bias between HCP and FCC in the bottom mode should be discussed because of the contradictory against the argument above [50]. According the current result, the mechanical stability plays an important role in distortion effect, while in the distortion free condition the packing history should be considered [50], i.e., the vibration protocols used in current work. To elaborate this point, different vibration modes were applied. Using amplitude $A = 0.1\ d$ and frequency $f = 50$ Hz as a reference, increasing amplitude ($A = 0.2\ d$) or frequency ($f = 70$ Hz) populates FCC particles, as exhibited in Fig. 8, except for D60 due to the aforementioned strong convection by large amplitude. This implies that high energy input benefits the growth of FCC in the bottom mode. Besides, in simulated colloidal systems [51, 52], the prevalence of HCP rather than FCC can also be identified when crystallisation initiated from walls. The identical two-dimension hexagonal packed layers (111) at the walls are considered as the main reason. The energetic favour of FCC may not be hold in these relatively two-dimensional scenarios, which requires further research to clarify the mechanical and energetic stability in the near-wall regions.

Apart from the wall effects, this less preference of FCC can partially be attributed to the internal packing fraction of the granular media ($\gamma_{\text{in}} \leq 0.67$) simulated in this work, which is smaller than that packing fraction (> 0.68) showing stronger preference of FCC [8]. As shown in Fig. 9, higher γ_{in} indeed leads more appearance of FCC particles generated from the bottom mode.

3.6 Influence of friction and comparison with experiments

The effect of the boundary geometry on the granular crystallisation has been demonstrated in frictionless media. It is necessary to clarify the influence of friction on

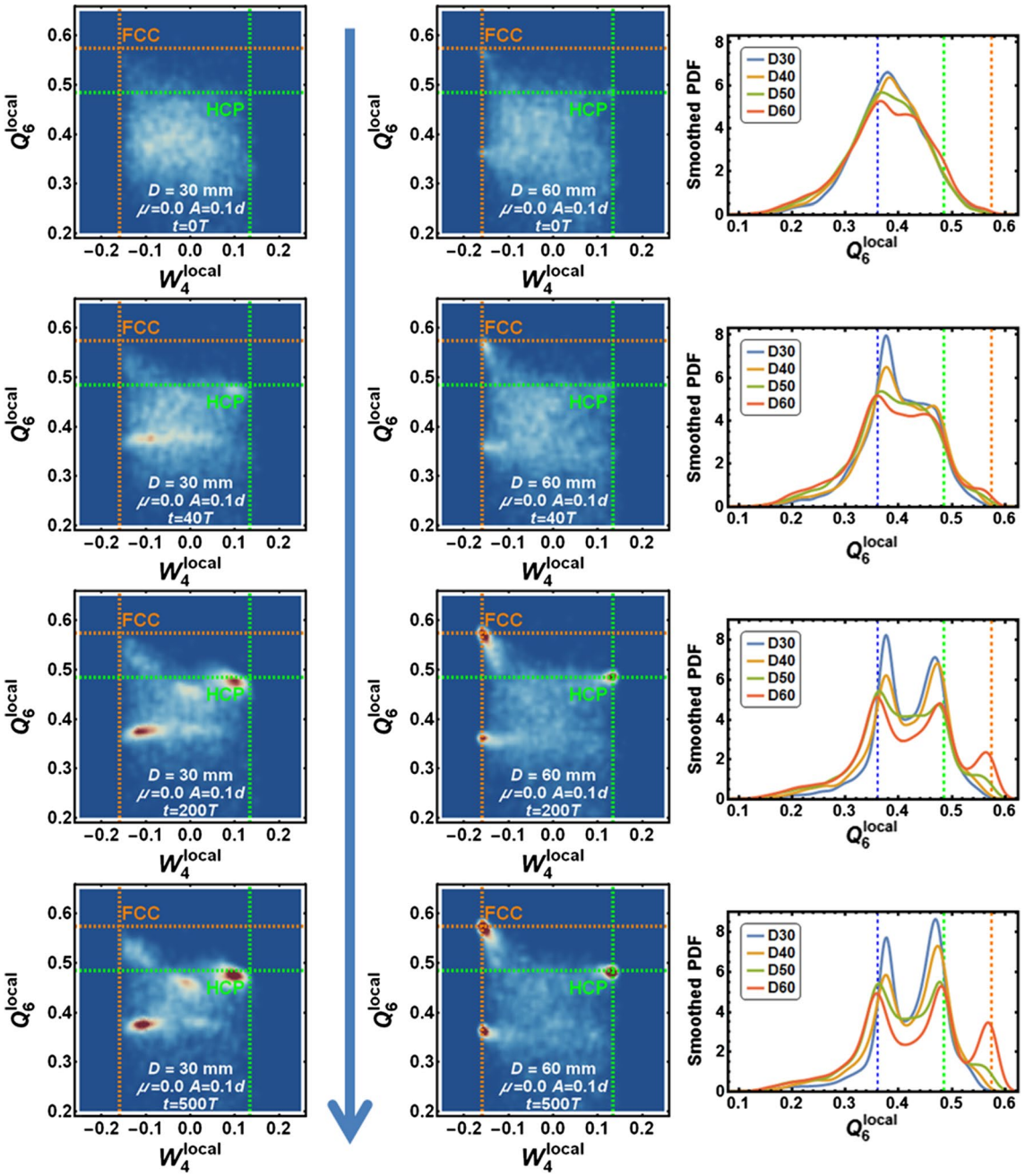

Fig. 6 Smoothed probability density histograms of the crystallised structures appearing in the granular media during vibration for D30 and D60. The (W_4^{local}, Q_6^{local}) coordinates are used to characterise the structure types. The intersects of pairs of dashed lines in orange and green are the coordinates of the FCC and HCP, respectively. The rightmost column gives the smoothed histograms of Q_6^{local} distributions in the granular media, with blue, green and orange dashed lines indicating wall hexagon units, HCP and FCC, repectively

crystallisation and compare it to available experimental data. Figure 10 shows for D30 the influence of friction on the evolution of the overall structural index F_6 during vibration. The initial state was kept identical for both the frictionless and frictional scenarios. The most obvious contrast between these two systems is the efficiency and degree of the granular crystallisation. The frictional energy losses between particles diminish the intensity of the vibration. Therefore, the crystallisation rate is lower in the frictional media and the required vibration time is longer to reach the final crystallised state. The simulated vibration duration (4000 periods for the longest vibration) is significantly shorter than the experimental study (40,000 periods for the longest vibration), but the result still matches quantitatively.

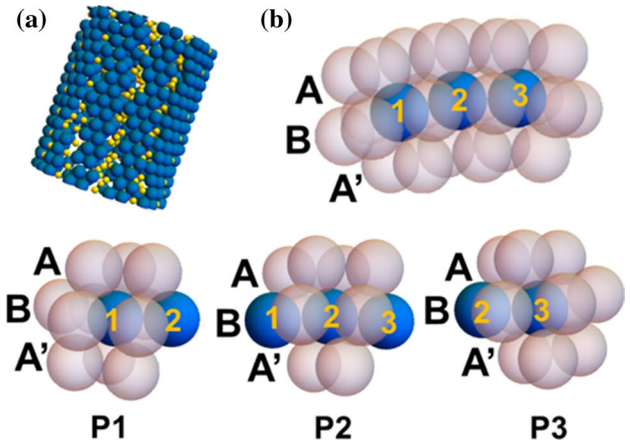

Fig. 7 Rupture in the HCP structure near the cylindrical wall in D30. **a** Blue particles are distorted HCP particles ($0.465 \le Q_6^{\text{local}} \le 0.505$, $W_4^{\text{local}} \ge 0.08$) while yellow particles are rupture particles ($0.465 \le Q_6^{\text{local}} \le 0.505$, $\left|W_4^{\text{local}}\right| \le 0.02$) with size scaled by 0.5 for visibility. **b** Typical rupture section with Particle 2 being the rupture particle. P1, P2, P3 are the 12-neighbour configurations of Particle 1, 2, 3, respectively (colour figure online)

Using the structural index obtained from the experimental results ($F_6 = 0.578$) as a benchmark, the orange dash line in Fig. 10, the corresponding transient snapshots in the simulation are extracted. Compared to the frictionless granular media, the frictional one exhibits similar S_6 density mapping, despite of the slight variation in radial expansion. Since the S_6 density mappings of different granular media match at the equivalent F_6, it is reasonable to argue that the structural evolution in the frictionless granular media represents a fairly complete crystallisation process for a given geometry. Hence, this morphological resemblance demonstrates that friction scarcely influences the mechanisms of the granular crystallisation and merely hinders the crystallisation growth. Based on this argument, the experiments can be considered as an intermediate state in the evolution of the frictionless granular media. Due to the frictional force, the granular medium in the experiment

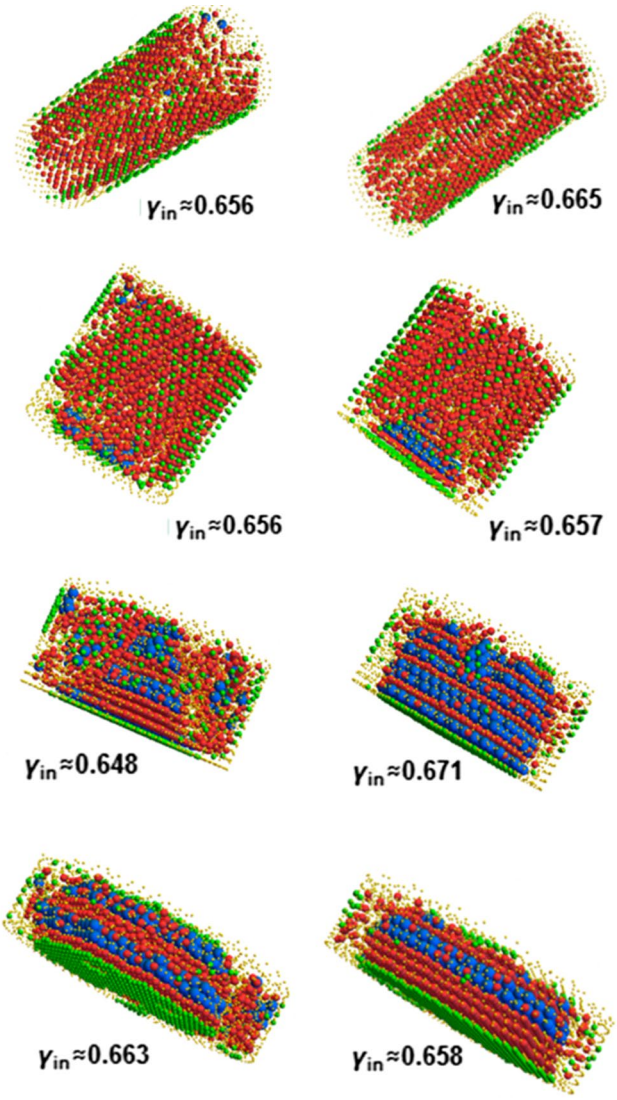

Fig. 9 The corresponding packing structures of individual particles dyed according to the (W_4^{local}, Q_6^{local}) coordinates in red-HCP, blue-FCC, green-surface hexagon and yellow-others. The diameters of the particles are rescaled for visualisation purposes. Left column-$A = 0.1$ d and right column-$A = 0.2$ d (colour figure online)

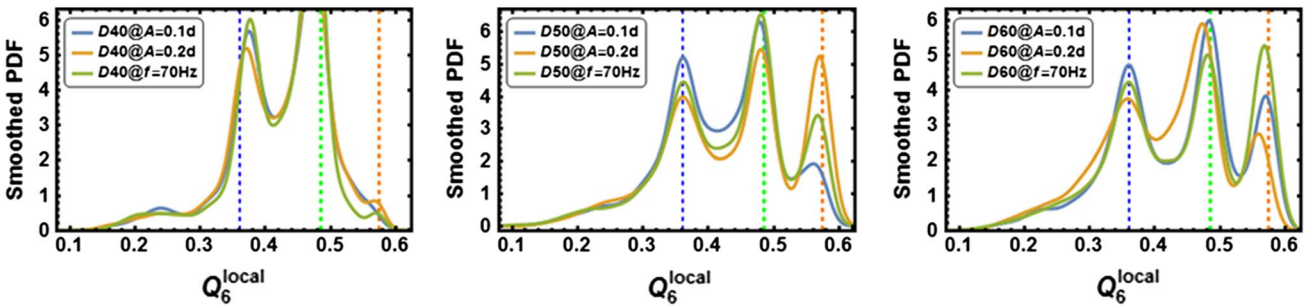

Fig. 8 Smoothed histograms of Q_6^{local} distributions of D40 (left), D50 (middle) and D60 (right) granular media subjected to different vibration modes. $A = 0.1$ d indicates 0.1 d amplitude and 50 Hz frequency; $A = 0.2$ d indicates 0.2 d amplitude and 50 Hz frequency; and $f = 70$ Hz indicates 0.1 d amplitude and 70 Hz frequency

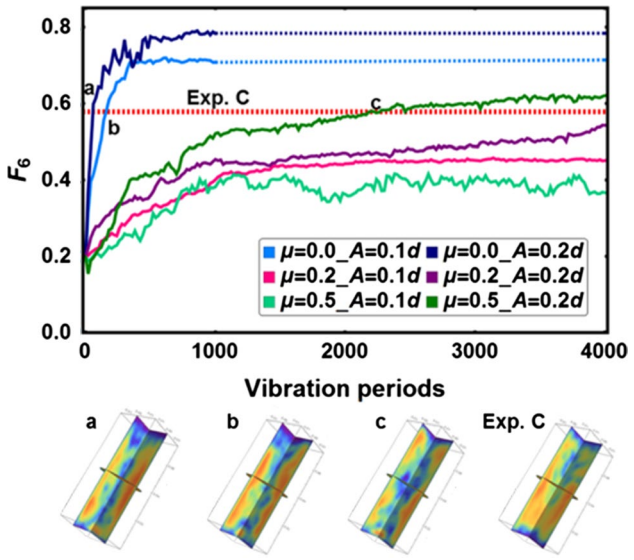

Fig. 10 Top-Evolution of the structural index F_6 of the frictionless and frictional granular media. The top two dashed lines serve as the extension for the final states in the simulation and the middle one labelled with Exp C represents the final state of the experiment performed with a vibration intensity $\Gamma = 2$ [31]. Bottom-S_6 spatial distributions of the labelled states in the simulated evolution and the experimental result. Friction coefficient (μ) and amplitude (A) values for the simulations are displayed in the legend of the Top graph

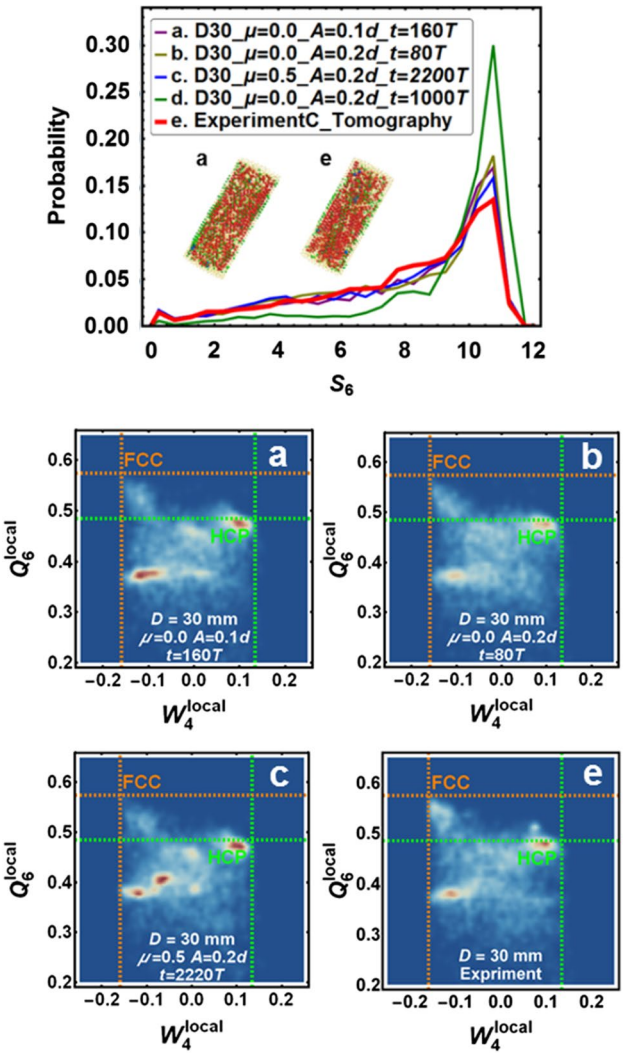

Fig. 11 Top-S_6 distributions of the final state in the Exp C in [31] and the transient states in the simulations. Particles dyed according to the (W_4^{local}, Q_6^{local}) coordinates are displayed as insets in the S_6 distribution in red-HCP, blue-FCC and green-surface hexagon. Bottom-The corresponding (W_4^{local}, Q_6^{local}) coordinate distributions. Friction (μ), amplitude (A) and duration (t) parameters for the simulations are displayed in the legend (colour figure online)

maintains the same granular crystallisation mechanisms although it is unable to reach the final state same as the frictionless simulations. It is noteworthy to mention that the merging crystalline regime at the bottom of the Exp C is the major difference between theory and experiment. This discrepancy is probably caused by the purely vertical vibration and shortened vibration duration in the simulations that ineffectively break the force chains sustaining the vertical perturbation.

The structural similarity between simulations and experiments is revealed by the S_6 distributions and the (W_4^{local}, Q_6^{local}) coordinate distributions as shown in Fig. 11. All the extracted transient states and the experimental result follow the same shapes of the S_6 distributions with the final state of the frictionless granular media presenting the highest peak magnitude. Similarly, the experimental medium forms two-dimensional hexagonal packing near the cylindrical wall and structures in a distorted HCP fashion. The prevalence of HCP over FCC in the cylindrical mode show little dependence on the friction condition according to Fig. 11.

The second set of comparisons is made for the relatively flat granular medium Exp D in [31], performed with $\Gamma = 2.8$ and resulted in $F_6 = 0.685$. Quantitative agreement is reflected by the different types of distributions used in this study. In addition, like the simulated result, the experiment presents only one crystallisation mode. With the elimination of the cylindrical wall crystallisation mode, the crystalline arrangement builds up from the bottom plane, and is characterised by the mixing of HCP and FCC planes. However, FCC is strongly favoured in experimental results of Exp D, according to Fig. 12. Since the packing history of Exp D, twice filling during vibration [31], is different from the simulation, it stresses that the packing history is one of the key factors determining the preference between FCC and HCP. On the other hand, by giving enough vibration intensity, the selection between FCC and HCP in the bottom mode still shows little dependency on the friction condition.

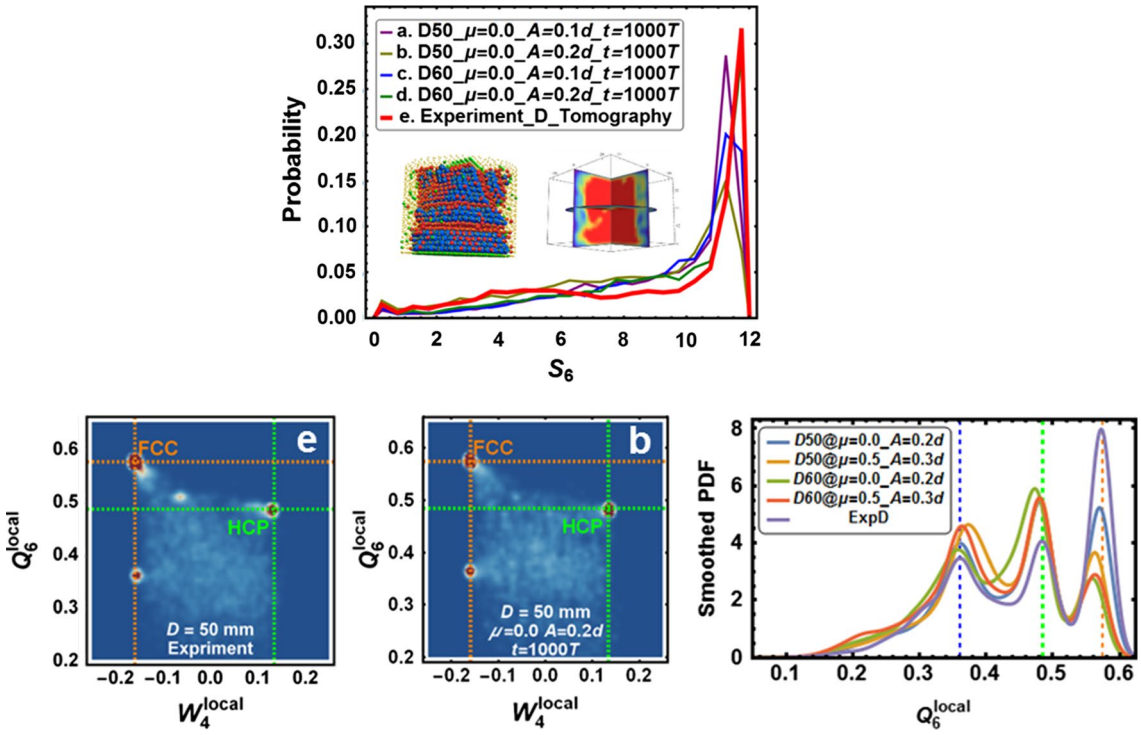

Fig. 12 Top-S_6 distributions of the final state in the experiment ExpD in [31] and the simulations along with the S_6 spatial distributions and dyed FCC/HCP particles of ExpD in the insets. Bottom-The corresponding (W_4^{local}, Q_6^{local}) coordinate distributions and the comparison of the smoothed histograms of Q_6^{local} distributions. Friction (μ), amplitude (A) and duration (t) values for the simulations are displayed in the legend

4 Conclusion

Granular crystallisation has been investigated from the entire system scale down to the individual particle scale in confined granular matter. The results clearly show that vibration naturally brings about a disorder-to-order transition, proving that crystallised structures are maintained during the transient evolution.

The crystallisation process and the role of the wall effect are explained by coarse-graining approach. Internal nucleation growth is restrained due to the purely repulsive interactions, and crystallisation from walls is preferential. The wall effect produces two-dimensional hexagonal packing as a growth template, but the following growth of crystalline arrays divides into a cylindrical mode and a bottom mode. In the cylindrical mode, the crystallised structure can be considered as a distorted HCP structure, while in the bottom mode, a mixture of HCP and FCC structure is identified. Depending on the geometry, D/d and H/D, competition between these two crystallisation modes falls into three phases during vibration. By increasing D, the bottom mode crystallisation gradually dominates, leading the crystalline regime to penetrating throughout the entire granular media in the axial direction. In the other case, i.e., when D decreases, the crystalline regions growing in the radial direction towards the axis are promoted from the cylindrical mode. Increasing the amplitude of vibration enhances the efficiency of the crystallisation and raises the competition level and leads to a sole crystallisation phase, which is commonly seen in experiments. However, the friction is found less important in determining crystalline structures, although it inhibits the crystallisation. Through the particle scale characterisation, we conclude that particles are driven to lodge themselves in structures with as many contacts as possible, because such structures provide sufficient collisions to dissipate kinetic energy and maintain the stability of the granular packing. The relationship between granular crystallisation and granular temperature is further explored and it is seen that granular crystallisation leads not only to structural but also to dynamic order.

In this study, granular crystallisation induced by vibration is proved to follow basic processes resulting in a predictable final structure. These results suggest that mechanical, thermal, electrical and other structure related effective properties can be modified by controlling vibration, motivating the continued study of granular crystallisation. Further research can be conducted to explore the physical mechanisms of inducing granular crystallisation. Meanwhile, this study shows the crystallisation can be

connected to the statistic description of granular matter. Thus, it would be interesting to seek more precise correlations between granular crystallisation and granular statistics.

Compliance with ethical standards

Conflict of interest The authors declare no conflict of interest.

References

1. Jaeger, H.M., Nagel, S.R.: Physics of the granular state. Science **255**(5051), 1523 (1992)
2. de Gennes, P.G.: Granular matter: a tentative view. Rev. Mod. Phys. **71**(2), S374–S382 (1999)
3. Wang, M., Pan, N.: Predictions of effective physical properties of complex multiphase materials. Mater. Sci. Eng. R Rep. **63**(1), 1–30 (2008)
4. Pouliquen, O., Nicolas, M., Weidman, P.D.: Crystallization of non-Brownian spheres under horizontal shaking. Phys. Rev. Lett. **79**(19), 3640–3643 (1997)
5. Carvente, O., Ruiz-Suárez, J.C.: Crystallization of confined non-Brownian spheres by vibrational annealing. Phys. Rev. Lett. **95**(1), 018001 (2005)
6. An, X., Yang, R., Dong, K., Yu, A.: DEM study of crystallization of monosized spheres under mechanical vibrations. Comput. Phys. Commun. **182**(9), 1989–1994 (2011)
7. Saadatfar, M., Takeuchi, H., Robins, V., Francois, N., Hiraoka, Y.: Pore configuration landscape of granular crystallization. Nat. Commun. **8**, 15082 (2017)
8. Shinde, D.P., Mehta, A., Barker, G.C.: Shaking-induced crystallization of dense sphere packings. Phys. Rev. E **89**(2), 022204 (2014)
9. Dong, K., Wang, C., Yu, A.: A novel method based on orientation discretization for discrete element modeling of non-spherical particles. Chem. Eng. Sci. **126**, 500–516 (2015)
10. Tai, S.-C., Hsiau, S.-S.: The flow regime during the crystallization state and convection state on a vibrating granular bed. Adv. Powder Technol. **20**(4), 335–349 (2009)
11. Mehta, A., Barker, G.C.: Vibrated powders: a microscopic approach. Phys. Rev. Lett. **67**(3), 394–397 (1991)
12. Ratnaswamy, V., Rosato, A.D., Blackmore, D., Tricoche, X., Ching, N., Zuo, L.: Evolution of solids fraction surfaces in tapping: simulation and dynamical systems analysis. Granul. Matter **14**(2), 163–168 (2012). https://doi.org/10.1007/s10035-012-0343-2
13. Barker, G.C., Mehta, A.: Transient phenomena, self-diffusion, and orientational effects in vibrated powders. Phys. Rev. E **47**(1), 184–188 (1993)
14. Zhao, J., Jiang, M., Soga, K., Luding, S.: Micro origins for macro behavior in granular media. Granul. Matter **18**(3), 1–5 (2016). https://doi.org/10.1007/s10035-016-0662-9
15. Richard, P., Nicodemi, M., Delannay, R., Ribiere, P., Bideau, D.: Slow relaxation and compaction of granular systems. Nat. Mater. **4**(2), 121–128 (2005)
16. Yu, A.B., An, X.Z., Zou, R.P., Yang, R.Y., Kendall, K.: Self-assembly of particles for densest packing by mechanical vibration. Phys. Rev. Lett. **97**(26), 265501 (2006)
17. Rosato, A.D., Dybenko, O., Horntrop, D.J., Ratnaswamy, V., Kondic, L.: Microstructure evolution in density relaxation by tapping. Phys. Rev. E **81**(6), 061301 (2010)
18. Philippe, P., Bideau, D.: Granular medium under vertical tapping: change of compaction and convection dynamics around the liftoff threshold. Phys. Rev. Lett. **91**(10), 104302 (2003)
19. Lan, Y., Rosato, A.D.: Convection related phenomena in granular dynamics simulations of vibrated beds. Phys. Fluids **9**(12), 3615–3624 (1997). https://doi.org/10.1063/1.869499
20. Carvente, O., Ruiz-Suárez, J.C.: Self-assembling of dry and cohesive non-Brownian spheres. Phys. Rev. E **78**(1), 011302 (2008)
21. Nahmad-Molinari, Y., Ruiz-Suárez, J.C.: Epitaxial growth of granular single crystals. Phys. Rev. Lett. **89**(26), 264302 (2002)
22. Panaitescu, A., Kudrolli, A.: Epitaxial growth of ordered and disordered granular sphere packings. Phys. Rev. E **90**(3), 032203 (2014)
23. An, X.Z., Yang, R.Y., Dong, K.J., Zou, R.P., Yu, A.B.: Micromechanical simulation and analysis of one-dimensional vibratory sphere packing. Phys. Rev. Lett. **95**(20), 205502 (2005)
24. Boutreux, T., de Geennes, P.G.: Compaction of granular mixtures: a free volume model. Phys. A **244**(1), 59–67 (1997)
25. Saadatfar, M., Kabla, A., Senden, T., Aste, T.: The geometry and the number of contacts of monodisperse sphere packs using X-ray tomography. In: Powders and Grains 2005-Proceedings of the 5th International Conference on Micromechanics of Granular Media 2005, pp. 33–36
26. Hanifpour, M., Francois, N., Robins, V., Kingston, A., Vaez Allaei, S.M., Saadatfar, M.: Structural and mechanical features of the order-disorder transition in experimental hard-sphere packings. Phys. Rev. E **91**(6), 062202 (2015)
27. Reimann, J., Brun, E., Ferrero, C., Vicente, J.: Pebble bed structures in the vicinity of concave and convex walls. Fusion Eng. Des. **98–99**, 1855–1858 (2015)
28. Francois, N., Saadatfar, M., Cruikshank, R., Sheppard, A.: Geometrical frustration in amorphous and partially crystallized packings of spheres. Phys. Rev. Lett. **111**(14), 148001 (2013)
29. Lumay, G., Vandewalle, N.: Experimental study of granular compaction dynamics at different scales: grain mobility, hexagonal domains, and packing fraction. Phys. Rev. Lett. **95**(2), 028002 (2005)
30. Komatsu, Y., Tanaka, H.: Roles of energy dissipation in a liquid–solid transition of out-of-equilibrium systems. Phys. Rev. X **5**(3), 031025 (2015)
31. Reimann, J., Vicente, J., Brun, E., Ferrero, C., Gan, Y., Rack, A.: X-ray tomography investigations of mono-sized sphere packing structures in cylindrical containers. Powder Technol. **318**(Supplement C), 471–483 (2017)
32. Russo, J., Tanaka, H.: The microscopic pathway to crystallization in supercooled liquids. Sci. Rep. **2**, 505 (2012)
33. Goodrich, C.P., Liu, A.J., Nagel, S.R.: Solids between the mechanical extremes of order and disorder. Nat. Phys. **10**(8), 578–581 (2014)
34. Kloss, C., Goniva, C., Hager, A., Amberger, S., Pirker, S.: Models, algorithms and validation for opensource DEM and CFD-DEM. Prog. Comput. Fluid Dyn. **12**(2–3), 140–152 (2012)
35. An, X.Z., Yang, R.Y., Zou, R.P., Yu, A.B.: Effect of vibration condition and inter-particle frictions on the packing of uniform spheres. Powder Technol. **188**(2), 102–109 (2008)
36. Steinhardt, P.J., Nelson, D.R., Ronchetti, M.: Bond-orientational order in liquids and glasses. Phys. Rev. B **28**(2), 784–805 (1983)
37. Kansal, A.R., Torquato, S., Stillinger, F.H.: Diversity of order and densities in jammed hard-particle packings. Phys. Rev. E **66**(4), 041109 (2002)
38. ten Wolde, P.-R., Ruiz-Montero, M.J., Frenkel, D.: Simulation of homogeneous crystal nucleation close to coexistence. Faraday Discuss. **104**, 93–110 (1996)
39. Goldhirsch, I.: Stress, stress asymmetry and couple stress: from discrete particles to continuous fields. Granul. Matter **12**(3), 239–252 (2010)

40. Weinhart, T., Thornton, A.R., Luding, S., Bokhove, O.: From discrete particles to continuum fields near a boundary. Granul. Matter **14**(2), 289–294 (2012)
41. Goldhirsch, I.: Introduction to granular temperature. Powder Technol. **182**(2), 130–136 (2008)
42. Hsiau, S.S., Lu, L.S., Tai, C.H.: Experimental investigations of granular temperature in vertical vibrated beds. Powder Technol. **182**(2), 202–210 (2008)
43. Rietz, F., Radin, C., Swinney, H.L., Schröter, M.: Nucleation in sheared granular matter. Phys. Rev. Lett. **120**(5), 055701 (2018). https://doi.org/10.1103/PhysRevLett.120.055701
44. Aste, T., Saadatfar, M., Senden, T.J.: Geometrical structure of disordered sphere packings. Phys. Rev. E **71**(6), 061302 (2005)
45. Tanaka, H.: Bond orientational order in liquids: towards a unified description of water-like anomalies, liquid-liquid transition, glass transition, and crystallization. Eur. Phys. J. E **35**(10), 113 (2012)
46. Berryman, J.T., Anwar, M., Dorosz, S., Schilling, T.: The early crystal nucleation process in hard spheres shows synchronised ordering and densification. J. Chem. Phys. **145**(21), 211901 (2016)
47. Rycroft, C.H., Grest, G.S., Landry, J.W., Bazant, M.Z.: Analysis of granular flow in a pebble-bed nuclear reactor. Phys. Rev. E **74**(2), 021306 (2006)
48. Nowak, E.R., Knight, J.B., Ben-Naim, E., Jaeger, H.M., Nagel, S.R.: Density fluctuations in vibrated granular materials. Phys. Rev. E **57**(2), 1971–1982 (1998)
49. Panaitescu, A., Reddy, K.A., Kudrolli, A.: Nucleation and crystal growth in sheared granular sphere packings. Phys. Rev. Lett. **108**(10), 108001 (2012)
50. Heitkam, S., Drenckhan, W., Fröhlich, J.: Packing spheres tightly: influence of mechanical stability on close-packed sphere structures. Phys. Rev. Lett. **108**(14), 148302 (2012)
51. Fujine, M., Sato, M., Katsuno, H., Suzuki, Y.: Effect of container shape and walls on solidification of Brownian particles in a narrow system. Phys. Rev. E **89**(4), 042401 (2014)
52. Arai, S., Tanaka, H.: Surface-assisted single-crystal formation of charged colloids. Nat. Phys. **13**(5), 503–509 (2017)